New Ventilation Cooling for Modular PM Machines Utilizing Flux Gaps and Rotor Ducts

W. Zhang[1], G. J. Li[1], *Senior Member, IEEE,* Z.Q. Zhu[1], *Fellow, IEEE,* B. Ren[2], and Y. C. Chong[2]
[1] Department of Electronic and Electrical Engineering, The University of Sheffield, Sheffield, UK, g.li@sheffield.ac.uk.
[2] Motor Design Ltd, an ANSYS company, 5 Edison Court, Wrexham Technology Park, Wrexham, LL13 7YT, UK

***Abstract*— This paper investigates a new ventilation cooling technology for modular permanent magnet (PM) machines. Air is pumped into the stator flux gaps and rotor ducts. A significant temperature reduction for the modular machines can be observed by introducing ventilated air. The flux gaps within the modular machines provide extra coolant path, notably modify the flow profile. Moreover, the flux gaps also provide additional contact area between machines and coolant, improving heat transfer rate. Comparative study between different machine configurations, including different inlet and outlet areas, different topologies of shaft, and different stator topologies have been investigated. Their influences on machine cooling have been investigated using computational fluid dynamics (CFD) modelling. Furthermore, since the coolant (air) will pass through the stator-rotor annular gap, i.e., airgap, as well as rotor ducts, the rotor speed will influence the cooling efficiency of the ventilation cooling system. This influence comes from shock loss, friction loss, and combining flow phenomenon. A series of experiments have been conducted to validate the CFD simulations.**

***Index Terms*— Combining flow, flux gaps, forced-air cooling, modular machine, ventilation cooling.**

I. INTRODUCTION

Permanent magnet (PM) machines have been used in a wide range of industry applications due to their high torque/power density and high efficiency. When any electrical machine (including PM machines) operates, heat will be generated inside it due to different types of losses. These include copper losses, iron losses, PM eddy current losses, and mechanical losses, etc. Heat generated inside the machine will result in temperature rise. Due to the maximum temperature limit of various materials, e.g., rare-earth metals such as PMs (≤ 150 ℃) and coil insulations (≤ 180 ℃), the machine temperatures should be limited to a certain range. To this end, employing an effective cooling systems is one of the solutions widely used for power dense electrical machine. It is well-established that heat transfers inside electrical machines through thermal conduction, convection and radiation due to temperature difference [1]. By employing the right cooling technologies, the heat transfer rate of the machine can be improved, and this helps to reduce temperature rise.

Various cooling technologies have been investigated in literature. Some of them are passive cooling methods that do not require extra pumps. Typical examples are potting materials filled in the end-space [2, 3]. Increasing contact surface area of frame or other machine components by using cooling fins [4] is another passive cooling method. Passive cooling technologies improve machine thermal performance without external power supply. However, compared with active cooling methods, the cooling efficiency of passive cooling methods is limited. Several active cooling methods have also been proposed in literature. One typical example is the forced-air cooling system. In these systems, fans can be located outside of the machines, such as the totally enclosed fan-cooled (TEFC) machine to improve the convection coefficient of the housing [5], or the through ventilation cooling machine [6] to directly dissipate heat from the heat generation components (e.g., windings, stator/rotor laminations and PMs). The fan can also be located inside the machines, such as on the surface of shaft or rotor [7]. In addition to the forced air cooling, other coolants can also be used, i.e., forced liquid cooling [8]. Some of these forced liquid cooling systems are direct forced liquid cooling [9, 10] and oil spray [6]. They are closed-circuit cooling systems, in which coolant is pumped into the machine. The coolant absorbs heat from the machine components and the surrounding circuit before transferring it to a heat exchanger. For direct forced liquid cooling, the coolant is in contact with the specific components, especially the coils and stator iron core. It can significantly reduce the temperature inside the machine. However, the risks of corrosion and liquid leakage should be considered. Other literature investigated indirect forced liquid cooling. The fluid channel can be assembled in the frame [11], the slot [12], the end-windings [13], the stator back-iron [14] or the shaft [15]. These fluid channels can remove heat near them effectively. Such indirect contact between the coolant and the machine components also avoids the corrosion issue presented in the direct forced cooling system. However, like the direct forced liquid cooling method, liquid leakage remains an issue that needs to be considered.

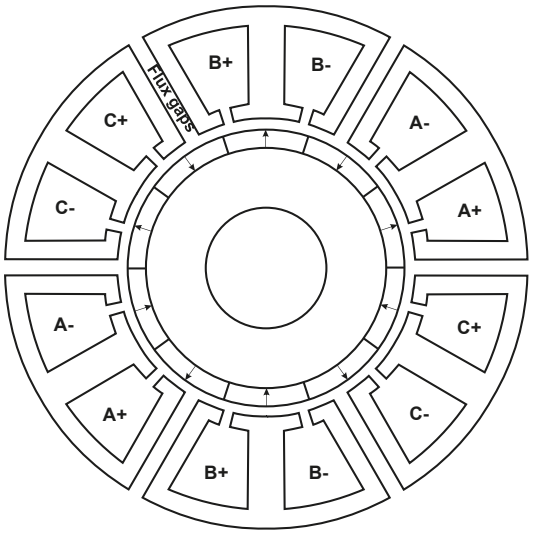

Fig. 1. Cross-section of modular machine.

For the modular machines, as shown in Fig. 1, a significant change in machine topology is introduced. According to the flow network analysis [16], the influence of the flux gaps on fluid dynamics and heat transfer can be significant. Different cooling methods for the PM machines with stator modularity have been investigated in literatures [10, 17, 18]. They indicated that introducing flux gaps/barriers into the machine stator can improve machine electromagnetic and thermal performances. The reason for improving the thermal performance is that, introducing flux gaps can not only increase the contact area between the stator and the coolant, but also significantly reduce the flow resistance of the whole cooling system for the investigated machines.

In this paper, a new ventilation cooling system will be employed for the modular machines and its non-modular counterpart. The influence of the flux gaps and rotor ducts on thermal performance of the modular machines will be investigated. In addition, the impact of other parameters such as the inlet and outlet areas, and the topology of shaft, will also be investigated. Moreover, the rotation of the rotor will lead to additional shock loss, friction loss, and combining flow phenomenon for ventilation cooling, resulting in higher system pressure loss. These have not been investigated in literature and will contribute to the novelty of this paper.

II. CFD Modelling and Machine Specification

A. CFD Modelling

The behaviour of fluid is governed by a set of nonlinear partial differential equations. Therefore, it is necessary to employ a CFD modelling to iteratively solve this problem. The CFD software package ANSYS-CFX has been used for this research. It is worth noting that the fluid flow in electrical machines is often considered as turbulent flow. Different simulation methods, i.e., direct numerical simulation (DNS), large eddy simulation (LES), and Reynolds-average Navier-Stokes (RANS) approach, can be employed to solve the turbulent flow problem. Compared with DNS and LES, RANS approach is more popular for the thermal analysis of electrical machines as it requires much less computational resources. Moreover, the shear stress transport (SST) k-ω model has been employed. Compared with other model, it makes the model stable in viscous-affected region (viscous sublayer), where the viscosity plays an important role in flow behaviour [19].

One of the key considerations for simulating fluid behaviour in electrical machines is the influence of rotor rotation. The rotor speed has a profound impact on the fluid velocity and pressure. To reduce the computational burden, the moving reference frame (MRF), also known as the "frozen rotor", is employed for steady-state analysis of the rotating machines. In the MRF approach, a mesh region for the rotating part acts as a reference frame, while the rest of the regions remain static. The reference frame is not moving physically, but the Coriolis force and centrifugal force caused by rotating is included in rotating reference frame. It is worth noting that, MRF approach can only simulate the time-average flow field, where the results calculated are highly dependent on the relative position of the rotating frame and static frame, or in other words, the initial rotor positions of the simulated electrical machines.

B. Machine Specification

A modular permanent magnet synchronous (PMSM) machine is used for the investigations in this paper, as shown in Fig. 2. The specifications of this machine are listed in Table I, which are the same for the non-modular machine. The average torques under rated current for the modular and the non-modular machine are 330Nm and 273Nm. respectively. For a fairer comparison and to show the improved cooling efficiency with flux gaps, the losses of both machines are kept the same.

The thermal properties of machine components are listed in Table II, and the properties of coolant are listed in Table III. It is worth noting that, the air is considered as incompressible fluid in simulations. To simplify the CFD modelling, a thermal anisotropy material is introduced for the coils to represent the mixture of copper and impregnation within stator slots. Hashin and Shtrikman approximation [20] in employed to calculate the anisotropic thermal conductivity of this material. The slot fill factor is assumed to be 0.4 for all the investigated machines and the conductivity that is vertical to the current direction is $0.65\,\mathrm{W/m/K}$, while the conductivity that is parallel to the current direction is $160\,\mathrm{W/m/K}$. The average density is $4269\ \mathrm{kg/m^3}$ and the average specific heat capacity is $1174\mathrm{J/kg/K}$.

Table I Parameters of Modular SPM Machine

Slot number	24	Rotor outer radius (mm)	129.4
Pole number	28	Stack length (mm)	210
Stator outer radius (mm)	154	DC voltage (V)	800
Flux gap width (mm)	10	Rated phase current (A)	$100/\sqrt{2}$
Airgap length (mm)	2	Number of turns per coil	10
Magnet thickness (mm)	6.6	Rated speed (rpm)	1500

Table II Properties of Machine Solid Components

	Housing	Rotor/Stator	Magnet	Shaft
ρ (kg/m^3)	2790	7650	7500	7800
λ (W/m/K)	168	30	7.6	52
c (J/kg/K)	833	460	7500	460

Noted: ρ, λ and c denote the density, thermal conductivity, and specific heat capacity, respectively.

Table III Properties of Air

Density (kg/m^3)	1.185
Thermal conductivity (W/m · K)	0.0261
Dynamic viscosity (Pa · s)	1.831×10^{-5}
Specific heat capacity (J/kg/K)	1.004×10^{3}

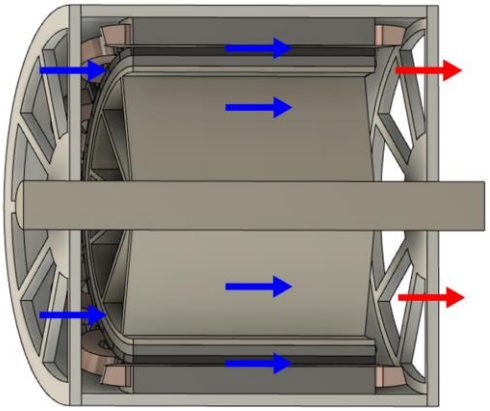

Fig. 2. Cut away view of the modular SPM machine with ventilation cooling.

TABLE IV-(A) TOPOLOGIES OF INVESTIGATED MACHINES

	M1	M2	M3	M4
Endcap	E1	E2	E2	E2
Shaft	SF1	SF1	SF1	SF1
Stator	Modular	Modular	Modular	Nonmodular
Sleeve	Yes	Yes	No	No

TABLE IV-(B) TOPOLOGIES OF INVESTIGATED MACHINES

	M5	M6	M7	M8
Endcap	E2	E2	E3	E3
Shaft	SF2	SF2	SF2	SF2
Stator	Modular	Nonmodular	Modular	Nonmodular
Sleeve	No	No	No	No

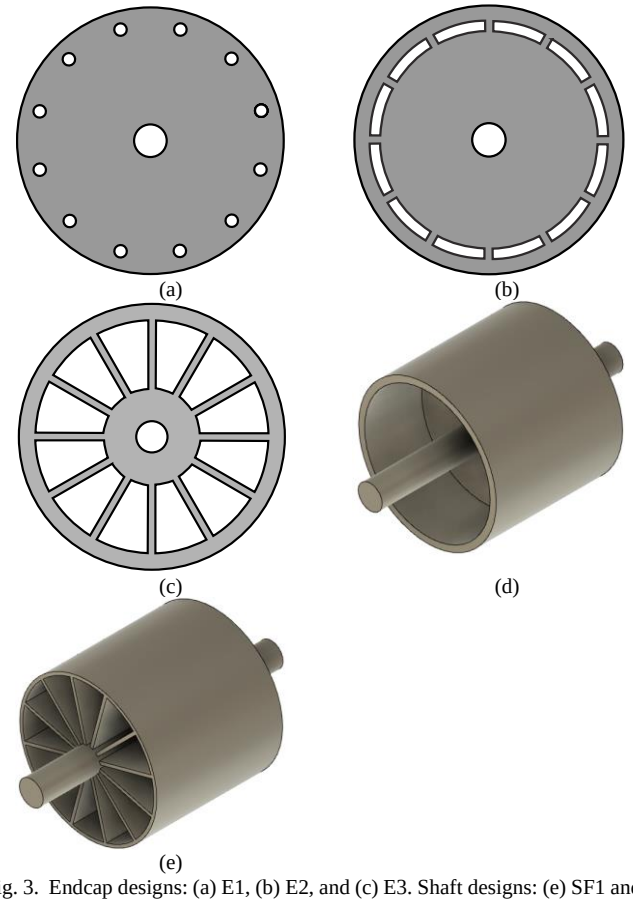

Fig. 3. Endcap designs: (a) E1, (b) E2, and (c) E3. Shaft designs: (e) SF1 and (f) SF2.

For comparative analyses, 8 machine models from model 1 to model 8, termed 'M1' to 'M8', as listed in Table IV, have been proposed and investigated. These models have different designs of endcaps, shafts, and stators. The topologies for endcaps and shafts are shown in Fig. 3. As described in Fig. 4, M1 is the original modular machine. M2 enlarges the cross-sectional area of the inlet and outlet of M1. For M1 and M2, the presence of a PEEK sleeve divides the machine into stator and rotor components. M3 omits the sleeve from M1 and M2. Once the sleeve is removed, the forced-air cooling system can also be adopted for the non-modular machines since the flux gaps are not the exclusive fluid path for the coolant. This leads to the development of M4, which has the same endcaps and shaft as those of M3 but with non-modular stator. A spoke-shape shaft can be used to provide additional coolant path for both modular and non-modular machines, termed M5 and M6, respectively. The further enlarged trapezoidal-shape inlet and outlet can be designed to align with the spoke-shape shaft, referred to as M7 and M8. Details of each machine component for different models are listed in Table IV-(A) and (B).

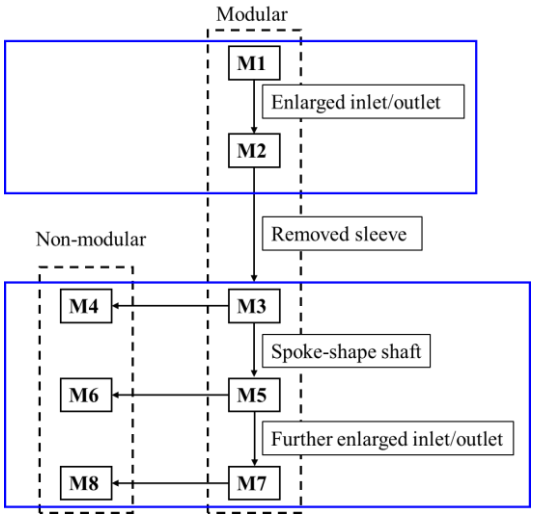

Fig. 4. The comparison between different models.

III. RESULTS AND DISCUSSIONS

Since the forced-air cooling system is employed, the temperature varying properties of air (especially the density and dynamic viscosity) can be neglected. In addition, the compressibility of air is also negligible. A uniform, fully developed airflow is introduced into the investigated modular machines with a mass flow rate of $0.48\,\mathrm{kg/s}$, and an inlet temperature of $20\,℃$. For the forced cooling systems, the gravitational effect has been neglected. Therefore, the circumferential symmetry of the modular SPM machine leads to a circumferentially symmetric distribution of flow field and heat transfer. Thus, a one-twelfth (30°) segment is simulated for 3D CFD modelling. It is worth noting that the axial domain lengths both upstream and downstream of the machine are around 2 times and 3.5 times the machine length to achieve a fully developed flow profile. This can prevent the model from having unwanted 'backflow' that can cause poor convergency and inaccurate results.

C. Comparative Analysis of Different Models

Fig. 5 shows the CFD results for M1. Since the flow rate is constant, a very high air velocity is reached due to the small inlet and outlet areas. This small area also leads to high pressure loss, which is 55.24kPa as shown in Fig. 6. Moreover, the stator components benefit from ventilated air, resulting in lower temperature, while the rotor component shows a much higher temperature in Fig. 5 (b) and (c). For example, the maximum winding temperature is $68.5\,℃$, while the maximum PM temperature is 110℃.

A design featuring non-circular inlet and outlet shape, as shown in Fig. 3 (b), has been adopted to enhance the performance of this cooling technology. This configuration is termed 'M2'. Compared with M1, the cross-sectional area has been increased from $174\,\mathrm{mm^2}$ to $728\,\mathrm{mm^2}$. A substantial reduction of dimensionless pressure loss coefficient for sudden expansions and contractions is achieved, leading to a significant reduction of pressure losses, as shown in Fig. 6.

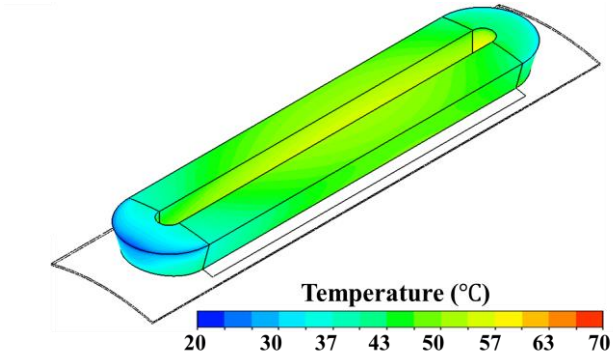

(a)

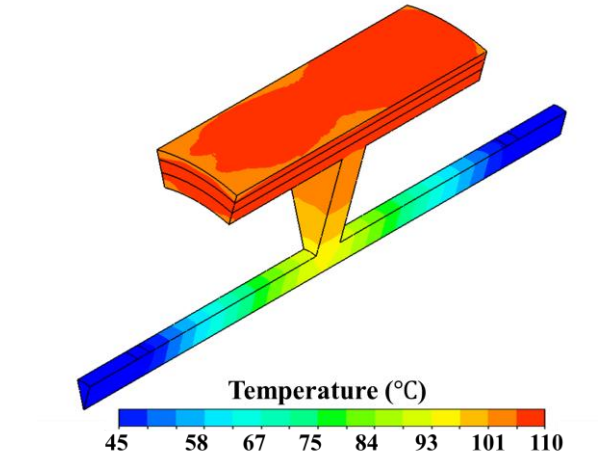

(b)

Fig. 5. (a) winding temperature distribution, and (b) rotor temperature distribution of M1.

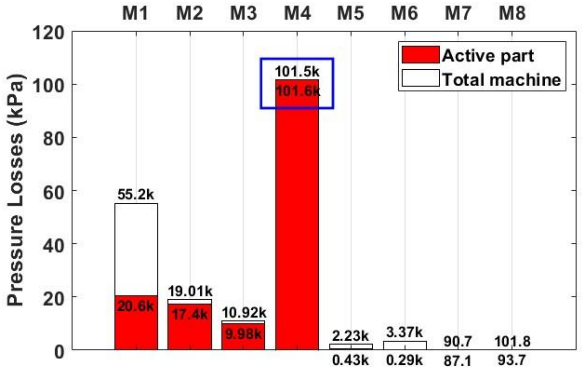

Fig. 6. Pressure losses for different machine configurations.

Moreover, when the PEEK sleeve is removed, the airgap can be used as an additional fluid path. This machine topology is termed 'M3'. A significant pressure reduction can be achieved, as shown in Fig. 6. In addition, after removing the sleeve, the coolant directly contacts the machine rotating components, especially the PMs. This results in a significant temperature reduction in rotor region, as shown in Fig. 7 (a), as well as a winding temperature reduction, as shown in Fig. 7 (b).

When the PEEK sleeve is removed, it is important to note that the machine's airgap can serve as an additional fluid path. As a result, non-modular machines can also employ ventilation cooling. This machine configuration is labelled 'M4'. However, it is worth mentioning that, at the same flow rate, the pressure loss of M4 is much higher than the other models, as shown in Fig. 6. Even though the airgap can offer a flow path, its small

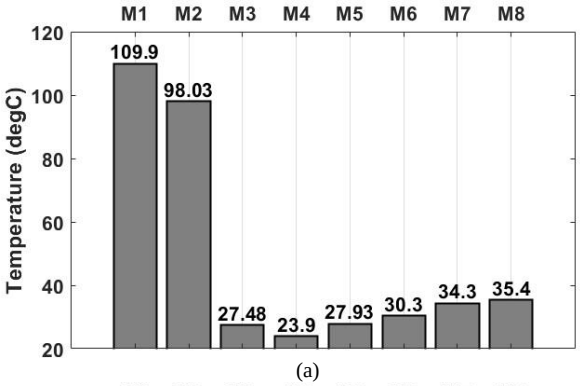

(a)

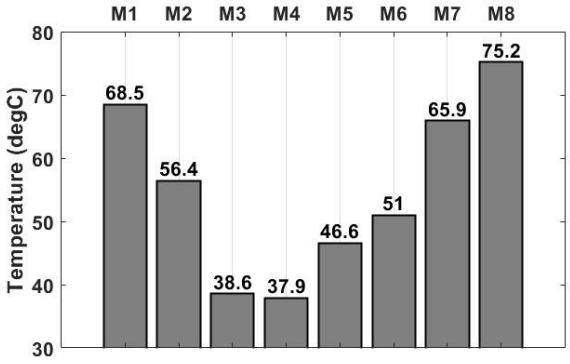

(b)

Fig. 7. (a) Maximum PM temperatures and (b) maximum winding temperature for different machine configurations.

cross-sectional area leads to an exceedingly high dimensionless pressure loss coefficient, resulting in substantial pressure losses. To be more specific, the pressure loss within the machine active part is 101.6kPa, slightly exceeds the total pressure loss between the inlet and outlet, as indicated by the blue box in Fig. 6. It illustrates that the narrower gaps result in a substantially lower absolute pressure within the machine's downstream part, causing air to be drawn back into the machine from the outlet.

The shafts for all previous designs (from M1 to M4) are disc-shaped and do not have holes for airflow as shown in Fig. 3 (e). However, this can be modified to a spoke shape, as shown in Fig. 3 (f). This spoke-shape shaft incorporates 12 spokes connecting the hub and the rotor, introducing an additional fluid path for both modular and non-modular machines. This design enhancement results in a substantial improvement in reducing pressure loss within the cooling system. For the modular machines with a spoke-shape shaft, they are termed 'M5'. For comparative analysis, the spoke shape shaft is also used in the non-modular machines, which is termed 'M6'. When compared to M3 and M4, both two topologies achieve an effective reduction in pressure losses, largely due to the introduction of rotor ducts, as shown in Fig. 6.

Additionally, the inlet and outlet areas can be extended to align with the rotating region, as shown in Fig. 3 (c). This leads to the development of new topologies for both the modular and non-modular machines, designated 'M7' and 'M8', respectively. These modifications result in a further reduction in pressure losses, as shown in Fig. 6. While the temperature reductions for these two configurations may not be as significant when compared to other machine topologies, their exceptionally low system dimensionless pressure loss coefficients allow for much higher flow rates, meeting the

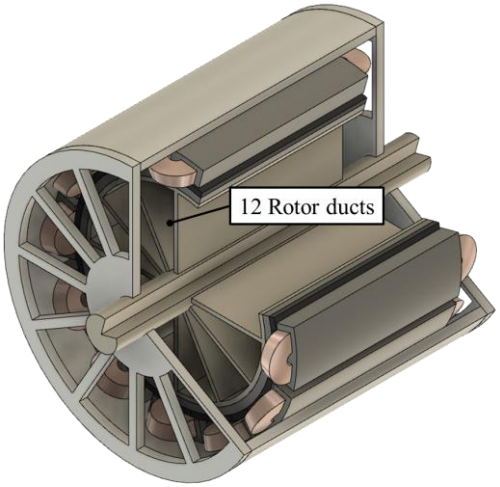

Fig. 8. Cut away view of M7.

requirements of external pumps. When considering the trade-off between the cooling efficiency and the requirement of pump pressure, it becomes evident that M7 and M8 exhibit the most optimal cooling performance. Further research in the following sections will be centred around these two machine configurations. The final design of M7 is shown in Fig. 8, which will be used for further investigations in the following sections.

D. Influence of Rotor Speed

As mentioned above, for the investigated non-modular machines with ventilation cooling, the flow paths for the ventilated air are mainly the airgap and rotor ducts (spoke-shape shaft). However, for the modular machines, the introduced flux gaps can be considered as additional stator ducts for the air flow. The influences of rotor speed on the flow resistances for those flow paths are essential. The rotor rotation introduces additional pressure losses because the direction of coolant is significantly changed when it enters the rotating ducts in the rotor iron core or shaft. This kind of pressure losses is named as shock losses [21]. In addition, the rotor rotation may also cause additional pressure loss due to friction loss variation and combining flow phenomenon [19].

The pressure losses in different machine regions versus rotor speed have been calculated using CFD models, as shown in Fig. 9. The results demonstrate that the pressure losses in the end-space inlet and the rotor ducts increase with increased rotor speed. It is noticed that the pressure losses in the airgap and flux gaps reduce when the rotor speed increases. This is caused by the combining flow phenomenon, which affects the pressure drop in the airgap and flux gaps.

As both the modular and non-modular machines use the same rotor ducts and inlets/outlets, one would expect that their pressure losses through the rotor ducts and end-space are similar. However, the simulated pressure losses in the airgap and flux gap are very much different. A significant pressure loss reduction is achieved after introducing the flux gaps. However, this reduction is less significant when the rotor speed increases. This is also caused by the combining flow phenomenon, which is another reason for the increased pressure loss in the machine cooling systems. The flow is deflected when it exits from the rotor ducts due to the centrifugal effect. The deflected flow will mix with the flow through the airgap (and the flow through the flux gaps for the modular machines). The flow separation at upstream and the flow combination at downstream result in additional pressure loss, which is named as combining flow loss. It is worth noting that, combining flow phenomenon only occurs in turbulent flow.

The flow velocity streamlines for the modular and non-modular machines at different rotor speeds are shown in Fig. 10 and Fig. 11. When the inlet volumetric flow rate is constant, the air velocity increases with rotor speed. The combining flow phenomenon will occur and aggravate with higher rotor speed. The combining flow also blocks the fluid flow in the flux gaps as shown in Fig. 11. When the machine is stationary, the air flows through the flux gaps, resulting in significant reduction in pressure loss. However, as the speed increases, the streamline in the flux gaps thins out. For example, the air barely flows through the flux gaps when the rotor speed is 3000rpm, as shown in Fig. 11 (c).

When the rotor is stationary or the rotor speed is relatively low, e.g., 1500rpm, the ventilated air passes through the flux

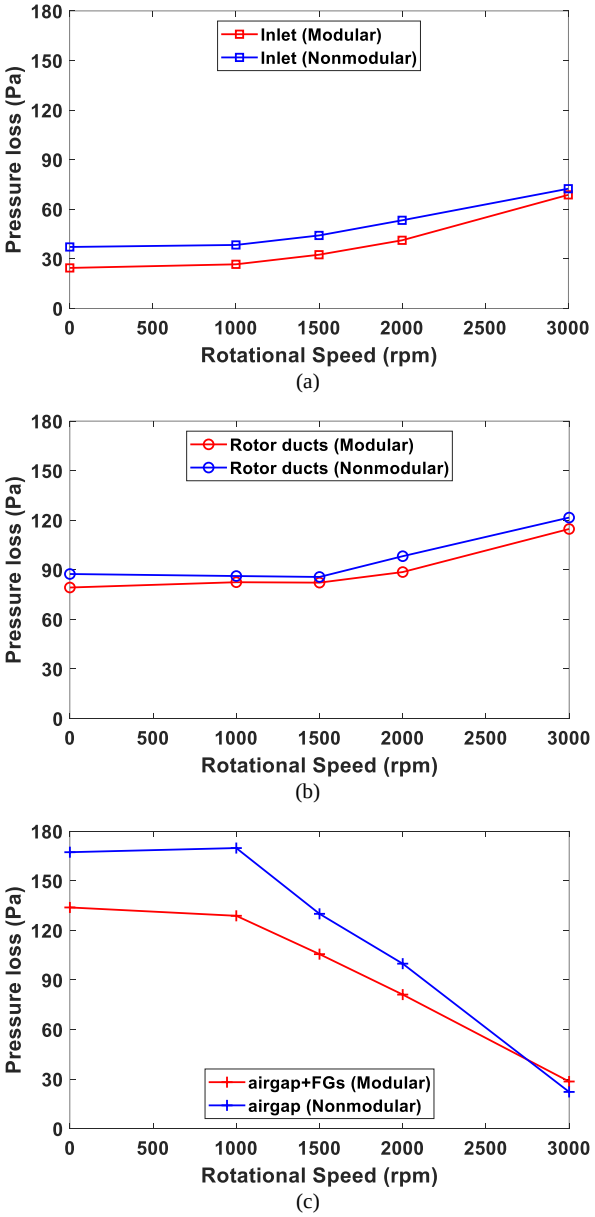

Fig. 9. Pressure losses in (a) end-space inlet region, (b) rotor ducts, and (c) airgap and flux gaps (for modular machines) *vs* rotor speed.

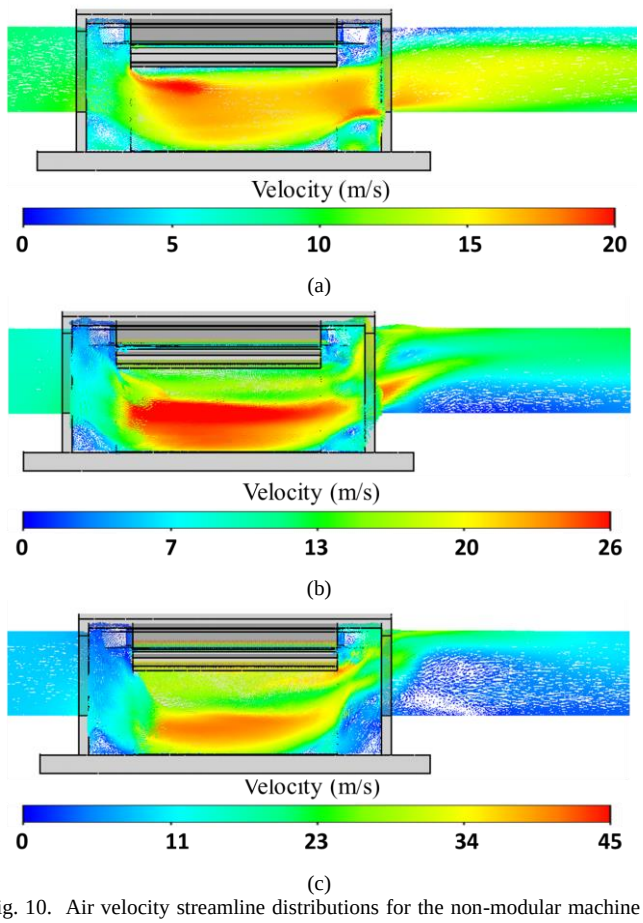

Fig. 10. Air velocity streamline distributions for the non-modular machine with different rotor speeds. Rotor speeds are (a) 0rpm, (b) 1500rpm, (c) 3000rpm.

gaps. However, at a higher rotor speed, i.e., 3000rpm, a combining flow phenomenon occurs, resulting in backflows in the flux gaps regions and blocking the fluid that flows through the flux gaps. This is the reason why air barely flows through the flux gaps when the rotor speed is 3000rpm.

IV. Experimental Validation

A. Tested Machines and Test Rig

To validate the predictions, a modular SPM machine with 2mm flux gaps, referred to as 'Modular 1' (as shown in Fig. 12), was fabricated and tested. The specifications of this machine are listed in Table V. To conduct a comparative analysis, its nonmodular counterpart, named 'Nonmodular' (obtained by inserting plastic sleeves into the flux gaps to block the airflow) was also tested to ascertain the influence of flux gaps on machine cooling.

Ventilation cooling experiments were performed using endcaps, as shown in Fig. 12 (a), equipped with 6 trapezoidal inlets and outlets. Furthermore, to evaluate the influence of inlet and outlet areas on machine cooling, instead of manufacturing new endcaps, two plastic sheets with smaller, round-shaped holes were devised to cover the endcaps. This alteration

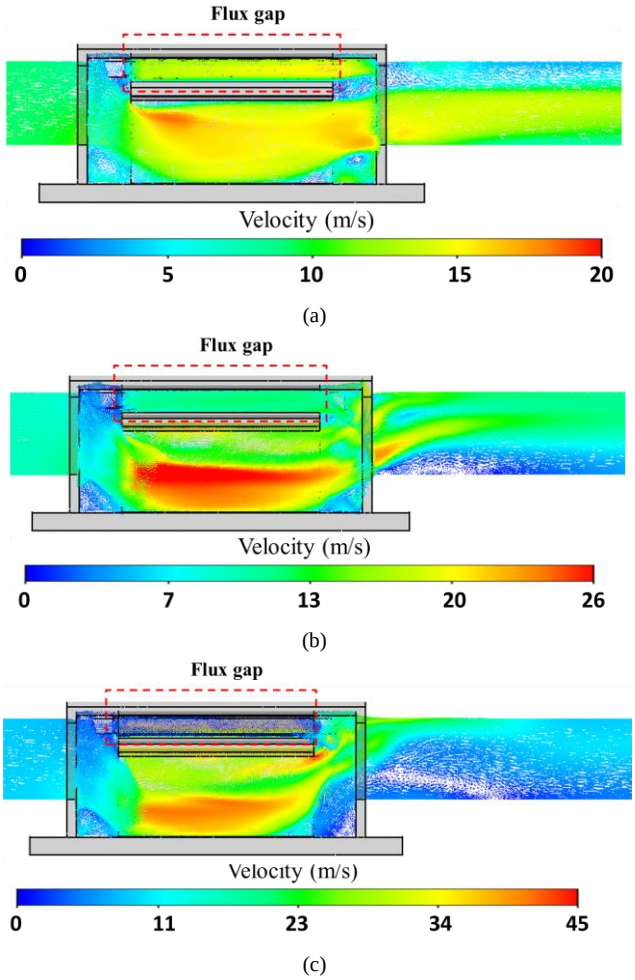

Fig. 11. Air velocity streamline distributions for the modular machine with different rotor speeds. Rotor speeds are (a) 0rpm, (b) 1500rpm, (c) 3000rpm.

established a reduced area for the inlet and outlet, denoted as 'Modular 2'.

TABLE V PARAMETERS OF PROTOTYPE MODULAR SPM MACHINE [17]

Slot number	12	Rotor outer radius (mm)	27.5
Pole number	14	Magnet thickness (mm)	3
Stator outer radius (mm)	50	Stack length (mm)	50
Stator inner radius (mm)	28.5	Rated phase current (A)	7.34
Flux gap width (mm)	2	Number of turns per coil	132
Airgap length (mm)	1	Rated speed (rpm)	400

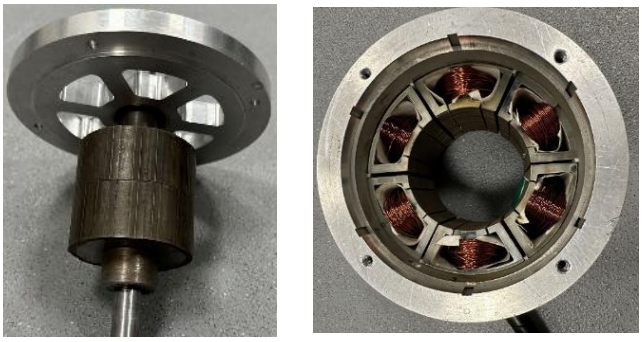

(a) (b)

Fig. 12. 12-slot/10-pole Modular SPM prototype machine. (a) Endcap and rotor, and (b) stator with stator modularity.

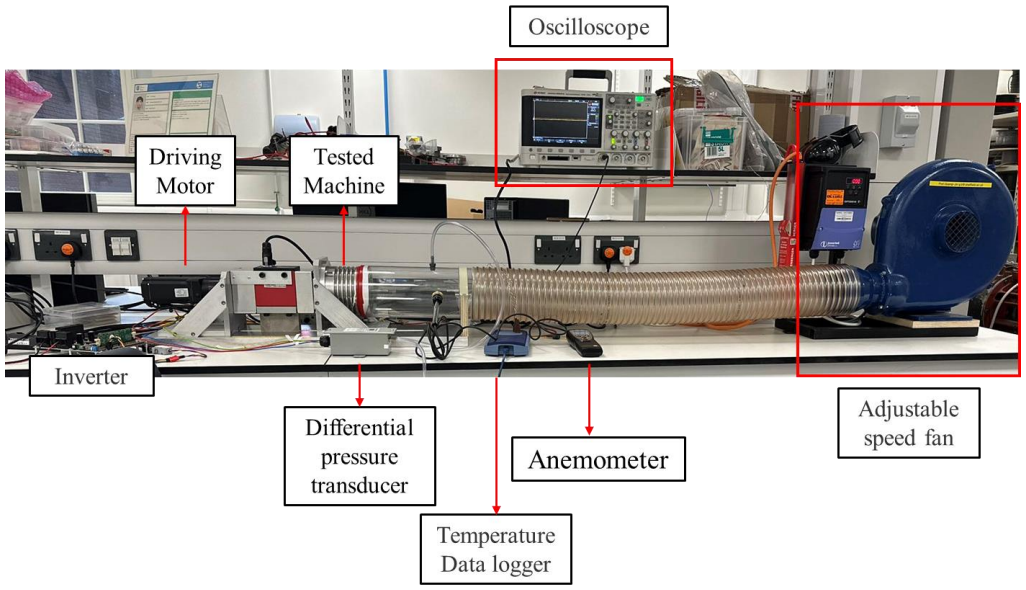

Fig. 13. Tested rig for ventilation cooling.

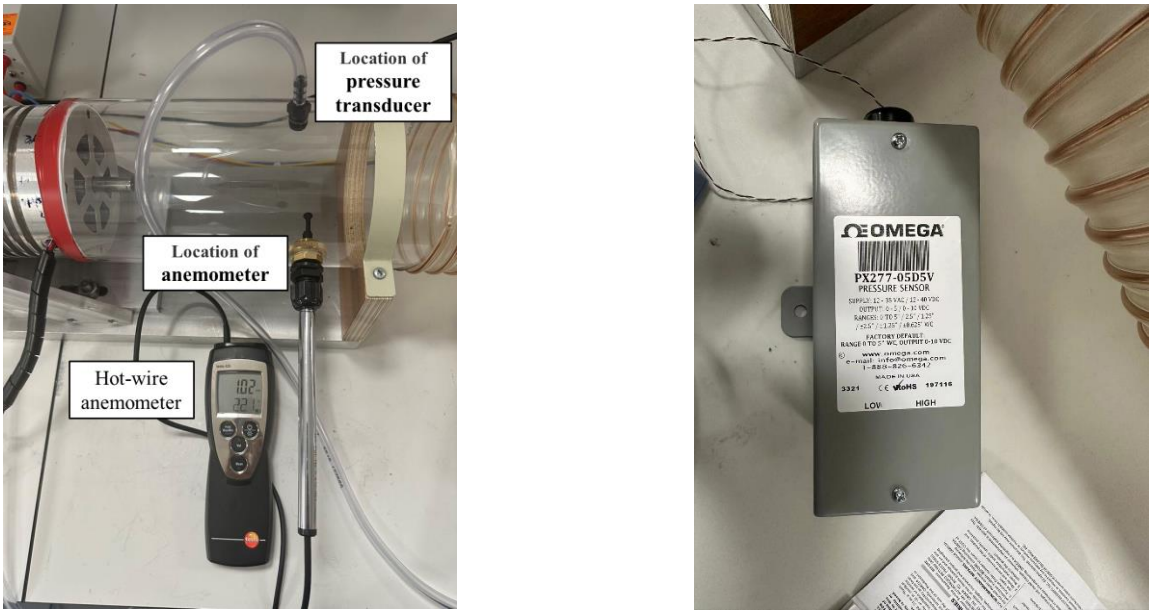

(a) (b)

Fig. 14. Measurement devices and their locations. (a) Hot-wire anemometer and (b) differential pressure transducer.

A ventilation cooling test rig, as shown in Fig. 13, has been built to validate the CFD simulations. The tested machine is driven by a dyno-motor, while ventilated air is produced by an adjustable speed fan. Essential parameters such as pressure losses, air velocity and machine temperatures are meticulously gauged using differential pressure transducer, hot-wire anemometer and T-type thermocouples, respectively. The adjustable speed fan is a centrifugal fan (L-28-E), manufactured by B.O.B Stevenson Ltd. At an ambient temperature of 20℃, the fan can provide a flow rate of $0.14 m^3/s$ at a static pressure of 500Pa. Its speed is controlled via an inverter, allowing for adjustable fan speeds ranging from 0rpm to 2500rpm.

Some measurement devices were incorporated for the ventilation cooling test. The differential pressure transducer, Omega PX277-05D5V, was utilized to measure the pressure variances between the upstream and downstream of the tested machines. The location of measured point for upstream flow is illustrated in Fig. 14 (a). The downstream pressure was maintained at ambient pressure (≈ 1 bar). The air velocity at upstream of the tested machine was determined using a hot-wire anemometer, with the specific measurement point shown in Fig. 14 (b). It is worth noting that, the hot-wire anemometer assesses gas velocity by detecting variation in the electrical resistance of its heated wire, which changes with the passage of gas through it. Moreover, the temperatures of coils in the tested machines were monitored using T-type thermocouples, and the recorded data was logged by a temperature data logger.

B. Measured Results

The air velocity for different machine configurations was measured at different fan speeds as shown in Fig. 15. The 'Modular 1' configuration, characterized by both flux gaps and larger trapezoidal inlet and outlet areas, exhibited higher air velocity compared to other machine configurations. However,

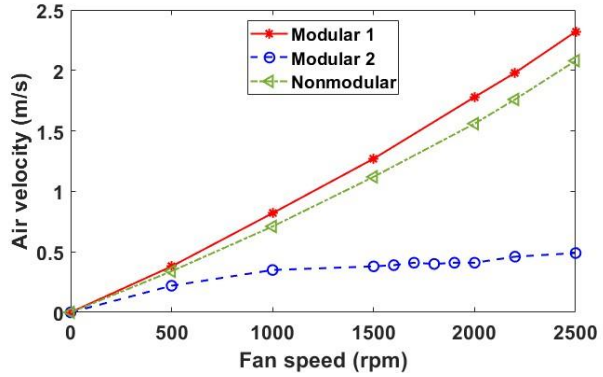

Fig. 15. Measured air velocity at different fan speeds.

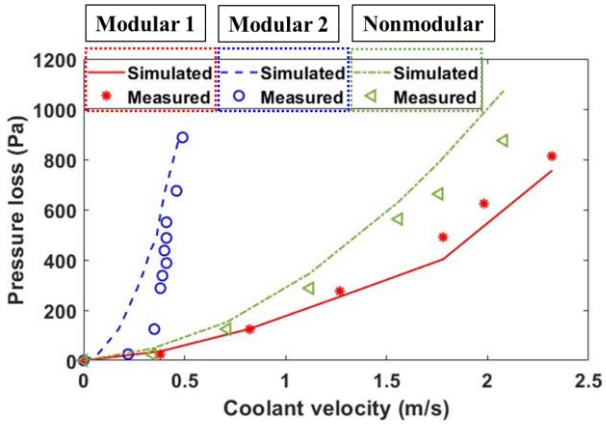

Fig. 16. Simulated and measured pressure losses for different machine stators and inlet and outlet area combinations.

upon inserting sheets within flux gaps, the air flow was obstructed, preventing it from passing through flux gaps. The system flow resistance is increased, resulting in a slightly lower air velocity. In addition, the measured result of 'Modular 2' showed a notably reduced air velocity. This reduction was attributed to very high flow resistance for this configuration, stemming from the reduction in the inlet and outlet area (reduced from 426.38mm^2 to 78.53mm^2).

The measured and simulated results of pressure losses for all machines at different air velocities are shown in Fig. 16. Observably, the pressure losses consistently increased as the air velocity increases. Under the same air velocity, the modular machine featuring larger inlet and outlet areas necessitates less pressure due to its reduced system flow resistance. However, it is important to highlight that due to the manufacturing tolerances, the sheets inserted within the flux gaps did not entirely fill the flux gaps, allowing for a slight passage of airflow. Therefore, the actual flow resistance for this candidate was lower than anticipated, leading to overestimated pressure losses in the simulation, as shown in Fig. 16. Moreover, discrepancies between the measured and simulated results were noticeable for Modular 2. This variance can be attributed to the accuracy limitations of the anemometer and differential pressure transducer. The discrepancy notably decreased with increased fan speeds.

The temperatures of various machine configurations are measured to compare with the simulated results, as shown Fig. 17 and Fig. 18. The simulated results indicated that without ventilation cooling, the machine temperature was around 186℃. However, upon the introduction of ventilated air, the machine temperature reduced significantly to around 50℃. Furthermore, consistently increased air velocity contributed to further reductions in machine temperature for both modular and nonmodular machines. Notably, a strong correlation between the measured and simulated results was evident. It is worth noting that, due to the passage of air resulting from manufacturing tolerances, the measured temperatures were slightly lower than expected, as shown in Fig. 18.

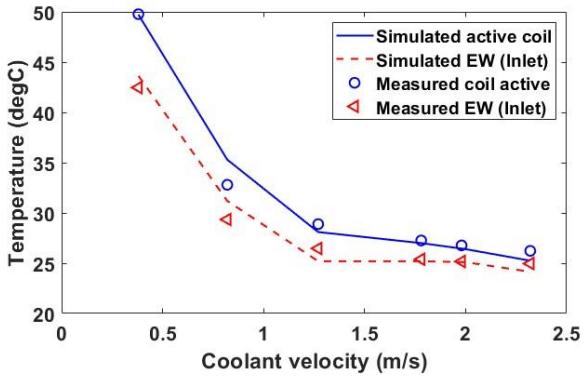

Fig. 17. Simulated and measured machine temperatures for Modular 1. It is worth noting that the temperature is 186℃ when coolant velocity is 0m/s.

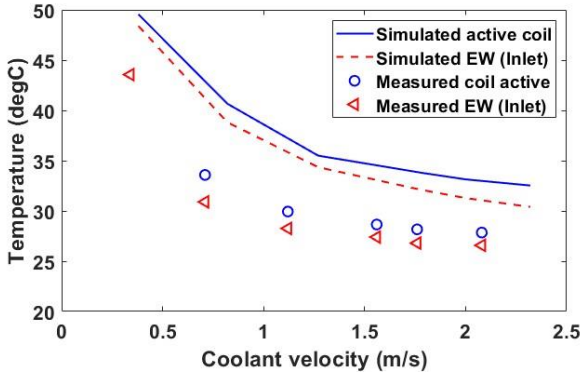

Fig. 18. Simulated and measured temperatures of 'Nonmodular'.

V. Conclusion

In this paper, a forced cooling technology, i.e., ventilation cooling, has been employed for the modular SPM machine and its non-modular counterpart. To investigate the cooling efficiencies of these technologies, and to understand the flow profiles and the heat transfers, a series of 3D CFD modelling has been carried out. The investigations revealed that the ventilation cooling system significantly reduces the machine temperatures. The influence of flux gaps on machine cooling has also been discussed. Due to their additional flow path, larger surface area of immersed solid, and lower flow resistance, the flux gaps result in lower pressure losses and reduced machine temperature for the modular machines. The influences of the cross-sectional area of the inlet and outlet for forced cooling technology have also been investigated. An increased cross-sectional area significantly reduces the dimensionless pressure loss coefficient caused by sudden expansions and contractions. It results in higher flow rate, and reduced machine temperature. Consequently, a larger cross-sectional area is preferred, provided that the mechanical reliability is not compromised.

The influence of rotor rotation on ventilation cooling efficiency has also been investigated. Due to additional pressure losses caused by shock and friction, a rotating machine results

in higher pressure loss compared to the stationary case. Increased rotor speed leads to higher pressure losses and may introduce the combining flow phenomenon in the machines with different coolant path. This phenomenon further increases the pressure losses for the entire machine cooling system. While the flux gaps in the modular machine result in lower pressure loss, the reduction of pressure loss is affected by the combining flow phenomenon. Thus, the benefits of flux gaps in improving cooling efficiency of ventilation cooling system may be diminished at higher rotor speed. The simulations and conclusions in this paper have been validated by tests.

Acknowledgement

This work is partially supported by the UK Engineering and Physical Science Research Council (EPSRC) under Grant No. EP/T017988/1 and partially sponsored by Motor Design Ltd, an Ansys company.

VI. REFERENCE

[1] Y. Gai, M. Kimiabeigi, Y. C. Chong, J. D. Widmer, X. Deng, M. Popescu, J. Goss, D. A. Staton, and A. Steven, "Cooling of automotive traction motors: Schemes, examples, and computation methods," *IEEE Trans. Ind. Electron.*, vol. 66, no. 3, pp. 1681-1692, 2018.

[2] M. Polikarpova, P. Ponomarev, P. Lindh, I. Petrov, W. Jara, V. Naumanen, J. A. Tapia, and J. Pyrhönen, "Hybrid cooling method of axial-flux permanent-magnet machines for vehicle applications," *IEEE Trans. Energy Conversion*, vol. 62, no. 12, pp. 7382-7390, 2015.

[3] S. Nategh, A. Boglietti, D. Barber, Y. Liu, and R. Brammer, "Thermal and manufacturing aspects of traction motors potting: A deep experimental evaluation," *IEEE Trans. Ind. electron.*, vol. 35, no. 2, pp. 1026-1035, 2020.

[4] S. Ulbrich, J. Kopte, and J. Proske, "Cooling fin optimization on a TEFC electrical machine housing using a 2-D conjugate heat transfer model," *IEEE Trans. Ind. electron.*, vol. 65, no. 2, pp. 1711-1718, 2017.

[5] S. Mizuno, S. Noda, M. Matsushita, T. Koyama, and S. Shiraishi, "Development of a totally enclosed fan-cooled traction motor," *IEEE Trans. Ind. Appli.*, vol. 49, no. 4, pp. 1508-1514, 2013.

[6] M. Popescu, D. A. Staton, A. Boglietti, A. Cavagnino, D. Hawkins, and J. Goss, "Modern heat extraction systems for power traction machines—A review," *IEEE Trans. Ind. Appli.*, vol. 52, no. 3, pp. 2167-2175, 2016.

[7] C. Micallef, S. J. Pickering, K. A. Simmons, and K. J. Bradley, "Improved cooling in the end region of a strip-wound totally enclosed fan-cooled induction electric machine," *IEEE Trans. Ind. electron.*, vol. 55, no. 10, pp. 3517-3524, 2008.

[8] D. Staton, E. Chong, S. Pickering, and A. Boglietti, *Cooling of Rotating Electrical Machines: Fundamentals, Modelling, Testing and Design*. IET, 2022.

[9] Z. Xu, A. La Rocca, P. Arumugam, S. J. Pickering, C. Gerada, S. Bozhko, D. Gerada, and H. Zhang, "A semi-flooded cooling for a high speed machine: Concept, design and practice of an oil sleeve," in *43rd Annu. Conf. IEEE Ind. Electron. Soc. (IECON)*, 2017: IEEE, pp. 8557-8562.

[10] R. Zhou, G. J. Li, Z. Q. Zhu, M. P. Foster, D. A. Stone, C. J. Jia, and P. McKeever, "Novel liquid cooling technology for modular consequent-pole PM machines," in *2021 IEEE IEMDC*, 2021: IEEE, pp. 1-7.

[11] R. Wrobel and B. Mecrow, "Additive manufacturing in construction of electrical machines–a review," in *2019 IEEE WEMDCD*, 2019, vol. 1: IEEE, pp. 15-22.

[12] G. Venturini, G. Volpe, and M. Popescu, "Slot water jacket cooling system for traction electrical machines with hairpin windings: Analysis and comparison," in *2021 IEEE IEMDC*, 2021: IEEE, pp. 1-6.

[13] V. Madonna, P. Giangrande, A. Walker, and M. Galea, "On the effects of advanced end-winding cooling on the design and performance of electrical machines," in *2018 XIII ICEM*, 2018: IEEE, pp. 311-317.

[14] X. F. Yang, A. Fatemi, T. Nehl, L. Hao, W. Zeng, and S. Parrish, "Comparative study of three stator cooling jackets for electric machine of mild hybrid vehicle," *IEEE Trans. Ind. Appli.*, vol. 57, no. 2, pp. 1193-1201, 2020.

[15] Y. Gai, M. Kimiabeigi, Y. C. Chong, J. D. Widmer, J. Goss, U. SanAndres, A. Steven, and D. A. Staton, "On the measurement and modeling of the heat transfer coefficient of a hollow-shaft rotary cooling system for a traction motor," *IEEE Trans. Ind. Appli.*, vol. 54, no. 6, pp. 5978-5987, 2018.

[16] D. A. Staton and A. Cavagnino, "Convection heat transfer and flow calculations suitable for electric machines thermal models," *IEEE Trans. Ind. electron.*, vol. 55, no. 10, pp. 3509-3516, 2008.

[17] A. Nollau and D. Gerling, "Novel cooling methods using flux-barriers," in *2014 ICEM*, 2014: IEEE, pp. 1328-1333.

[18] R. Zhou, G. J. Li, Z. Q. Zhu, M. P. Foster, and D. A. Stone, "Improved cooling in modular consequent pole PM machine utilizing flux gaps," in *2020 IEEE ECCE*, 2020: IEEE, pp. 4253-4260.

[19] Y. C. Chong, "Thermal analysis and air flow modelling of electrical machines," Ph.D. dissertation, Dept. Mech. Eng., Edinburgh Univ., Edinburgh, U.K., 2015.

[20] N. Simpson, R. Wrobel, and P. H. Mellor, "Estimation of equivalent thermal parameters of impregnated electrical windings," *IEEE Trans. Ind. Appli.*, vol. 49, no. 6, pp. 2505-2515, 2013.

[21] J. D. Webb, "The flow of air through axial cooling ducts in a rotor," *The English Electric Company Ltd. Department Mechanical Engineering Laboratory, Whetstone, Report No. W/M (2A) p*, vol. 85, 1964.